Iranian Journal of Physics Research, Vol. 21, No. 3, 2021

Properties of 132Xe Neutral Atoms Scattering for 165K and 275K Temperatures

A Nawaf Akour
Department of Basic Science, Al-Huson College, Al-Balqa Applied University, Salt, Jordan

E-mail: abd-akour@bau.edu.jo

(Received 22 July 2019 ; in final form 08 November 2020)

Abstract
This work aims to use an important method Galitskii-Migdal-Feynman (GMF) for diatomic molecules $^{132}Xe_2$, to calculate the effective phase shifts which are then used to compute the effective total and viscosity cross sections at low density and temperature . this study has shown that it's crucial to include partial waves up to $\ell = 14$; for $\ell > 14$, the effect of the potential becomes negligible . Comparing with partial waves cross sections we deduce that the cross section is dominated by S-wave scattering for low energy (wave number k < 0.1 $Å^{-1}$), otherwise D and G partial waves dominate . The highest peak rises from the partial effective D and G-wave resonance, where the system sustains a quasi-bound state trapped by the $\ell = 2, 4$ centrifugal barrier. The average cross section is also determined.

Keywords: Effective Total Cross Section, Effective Phase Shifts, Effective Viscosity Cross Section, Galitskii-Migdal-Feynman Formalism, 132Xe Gas

1. Introduction

This research sheds light on scattering properties of ^{132}Xe gas for 165K and 275K temperatures within a generalized scattering framework; based on the Galitskii-Migdal–Feynman (GMF) formalism [1]. The GMF formalism was firstly improved for the Fermions many-body systems and then extend to the many body Bose systems [2, 3, 4]. The most significant of this research that it's built from the initial basic concepts a complementary microscopic assumption for xenon dimer (^{132}**Xe**) gas system, using GMF method with interatomic pair potential as the main input. However there are many studies on scattering other spices with xenon such as electron xenon scattering cross section [5, 6], proton xenon scattering cross section [7] , and neutron xenon scattering cross section[8], but studies on neutral xenon particle are rare [9, 10] scattering properties. This study is a unique one not only for integrated microscopic assumptions used for the first time on xenon but also for its specified small range in temperature and momentum where quantum interactions and resonance appear.

We first use a matrix-inversion technique to solve GMF integral equation and then compute the effective relevant phase shifts in the medium (which is the most important GMF processing product) in order to investigate the effective ^{132}Xe -^{132}Xe cross sections. The basic input used is the acclaimed interatomic xenon potential, namely, HFD-B2 [11] which is considered the closest to the actual ^{132}Xe -^{132}Xe potential.

Several potentials suggested approaching the actual xenon potential and other rare gasses [12]. Pade Approximants used to determine upper and lower bounds to the Van der Waals C_6, C_8 and C_{10} coefficient of noble gasses[13], krypton and xenon have been simulated using several potentials [14]. For xenon the semi-empirical gives more acceptable results comparing with experimental ones.

Molecular dynamics were used to study the transport properties of Bose gasses (such as Ne, Ar, Kr and Xe) and the results agree well with experimental results [15].

Absolute total elastic cross sections for Xe-Xe collisions have been computed for collision energies from 0.01 eV to 10 keV [16]. This result implements the information previously obtained from the Xe_2 interaction potential.

The rest of the paper is organized as follows. Section 2 presents the material and method. The results of effective cross sections properties are performed and shown in Section 3. Finally, in Section 4, the paper is concluded with some closing remarks.

2. Material and method

Natural units are used such that; m of xenon (m = 131.3 au, m^*=0.68m)[17]; k_B, $\hbar$ ($=h/2\pi$). The conversion factor is

$$\frac{\hbar^2}{2m^*} = 0.5404 \text{ K.Å}^2. \quad (1)$$

2.1 GMF T-matrix

The first step is to determine δ_ℓ^E by solving the GMF integral equation, using a matrix-inversion technique. The GMF formalism will be summarized shortly such that the quantities used are defined for reference purposes, since it is described briefly elsewhere [18, 19]. The GMF T-matrix is the main significant quantity in this formalism which really transformed the effective interaction of two-body into momentum space. Otherwise, it can be expressed as generalized scattering amplitude or a 'dressed' Lippmann-Schwinger t-matrix (which describes two-body scattering in *free* space). It is given by [19, 2**Error! Bookmark not defined.**]

$$T\left(\vec{p},\vec{p}';s,\vec{P}\right) = u\left(\left|\vec{p}-\vec{p}'\right|\right) - (2\pi)^{-3}\int d\vec{k}u\left(\left|\vec{p}-\vec{k}\right|\right) \times\left[g_0(k,s)Q\left(\vec{k},\vec{P},\beta\right) - g_0^+(k,s)\bar{Q}\left(\vec{k},\vec{P},\beta\right)\right] T\left(\vec{k},\vec{p}';s,\vec{P}\right). \quad (2)$$

Here:

The operator $u \equiv \frac{2m_r V}{\hbar^2} \equiv \frac{1}{2}V$ [in natural units], $m_r = \frac{1}{2}m$ for ^{132}Xe interacting pair, V the Fourier transform of a static central two-body potential, V(r). The parameter s is given by

$$s \equiv 2m_r\left(2P_o - \frac{P^2}{m}\right) \quad (3)$$

where P_0 is the total energy of the pair, P^2 is the energy carried by the center of mass.

The input single-particle energy spectrum can be approximated by the free-particle energy $\varepsilon(k) = \frac{\hbar^2 k^2}{2m}$; so [in natural units]

$$\varepsilon = k^2 \quad (4)$$

To be more precise, this approximation is valid for the ideal gas only. The implication is that the so-called 'self-energy insertion' is neglected here. The incorporation of this insertion into our framework would necessitate a rather lengthy self-consistent calculation.

The effective phase shifts $\delta_\ell^E(p;P,\beta)$ can be determined by parameterizing the on- energy-shell T-matrix as follows:

$$\tan\left(\delta_\ell^E(p;P,\beta)\right) \equiv \frac{\mathrm{Im}T_\ell(p;P;\beta)}{\mathrm{Re}T_\ell(p;P;\beta)} \quad (5)$$

$\mathrm{Im}T_\ell(p;P;\beta)$ and $\mathrm{Re}T_\ell(p;P;\beta)$ denote, respectively, the imaginary and real parts of $T_\ell(p;P;\beta)$; they are defined by

$$\mathrm{Re}T_\ell(p;P;\beta) = -\frac{2\pi}{p\left(Q(p;P,\beta)+\bar{Q}(p;P,\beta)\right)\sin\left(2\delta_\ell^E(p;P,\beta)\right)} \quad (6)$$

$$\mathrm{Im}T_\ell(p;P;\beta) = -\frac{2\pi}{p\left(Q(p;P,\beta)+\bar{Q}(p;P,\beta)\right)\left(1-\cos\left(2\delta_\ell^E(p;P,\beta)\right)\right)} \quad (7)$$

where $Q(\bar{Q})$ is the related to the probabilities of a transition into (out of) states $\left|\vec{k}-\vec{P}\right\rangle$ and $\left|\vec{k}+\vec{P}\right\rangle$; these operators are given by [20, 21].

$$Q(k,P,\beta) = \left(1+n\left(\left|\vec{k}-\vec{P}\right|\right)\right)\left(1+n\left(\left|\vec{k}+\vec{P}\right|\right)\right); \quad (8)$$

$$\bar{Q}(k,P,\beta) = n\left(\left|\vec{k}-\vec{P}\right|\right)n\left(\left|\vec{k}+\vec{P}\right|\right), \quad (9)$$

V(r) used as the HFD-B2 potential [11], which is generally preferred as the most reliable potential formula of Xe-Xe interaction. This is given by

$$V(r) = \varepsilon V^*(x) \quad (10)$$

Where,

$$V^*(x) = A\exp\left(-\alpha x + \beta x^2\right) - \left\{\frac{C_6}{x^6}+\frac{C_8}{x^8}+\frac{C_{10}}{x^{10}}\right\}F(x); \quad (11)$$

And,

$$F(x) = \begin{cases}\exp\left[-\left\{\frac{D}{x}-1\right\}^2\right], & x < D \\ 1, & x \geq D\end{cases} \quad (12)$$

$$x \equiv \frac{r}{r_m};$$

$D = 1.114$; $A = 5.44087277\times10^4$;
$\alpha = 7.52958289$; $\beta = -3.330428$;
$C_6 = 1.00555220$; $C_8 = 0.58359858$;
$C_{10} = 0.47378306$; $\varepsilon = 282.8\,K$;
$r_m = 4.3656Å$.

$$g_0\left(\vec{k},s\right) \equiv \frac{1}{k^2 - s - i\eta}, \quad (13)$$

is the free Green's function, η being a positive infinitesimal in the scattering region and zero otherwise.

2.2 Effective cross sections

The effective total σ_T and viscosity σ_η cross sections for our many-bosonic system are given by

$$\sigma_T = \frac{8\pi}{k^2}\sum\nolimits_{\ell=even}(2\ell+1)\sin^2\left(\delta_\ell^E(k)\right) \quad (14)$$

$$\sigma_\eta = \frac{4\pi}{k^2}\sum_{\ell=0}^{\infty}\frac{(\ell+1)(\ell+2)}{\left(\ell+\frac{3}{2}\right)}\left(1+(-1)^\ell\right)\sin^2\left(\delta_{\ell+2}^E(k)-\delta_\ell^E(k)\right) \quad (15)$$

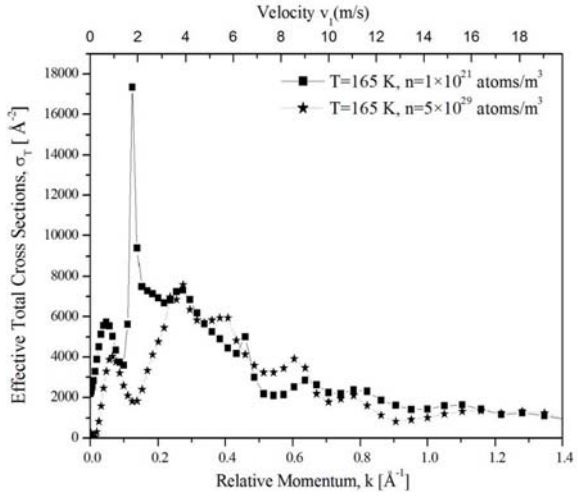

Figure 1. The effective total cross section σ_T [Å^2] for ^{132}Xe-^{132}Xe scattering as a function of relative momentum k [Å^{-1}] at temperature T = 165 K for different number densities n

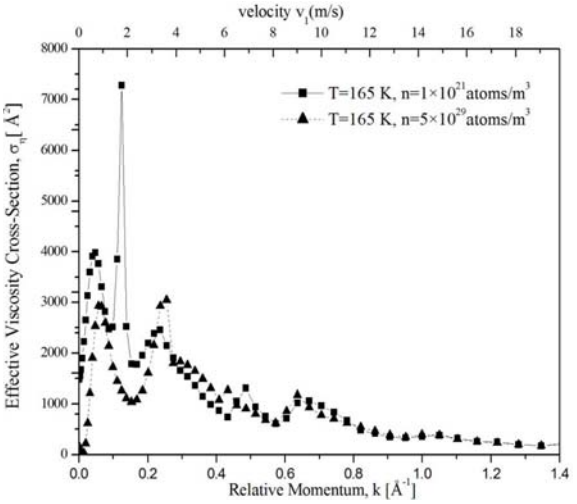

Figure 2. The effective viscosity cross section σ_η [Å^2] for ^{132}Xe-^{132}Xe scattering as a function of relative momentum k [Å^{-1}] at temperature T = 165 K for two different number densities n

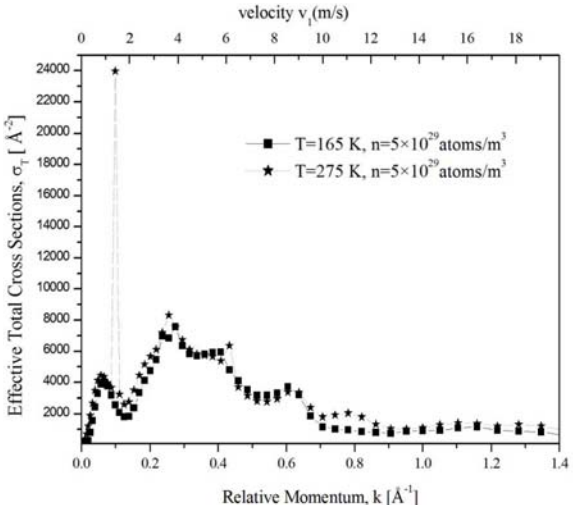

Figure 3. The effective total cross section σ_T [Å^2] for ^{132}Xe-^{132}Xe scattering as a function of relative momentum k [Å^{-1}] at temperature T = 165 K and 275 K for number density n = 5× 10^{29} atoms/m^3

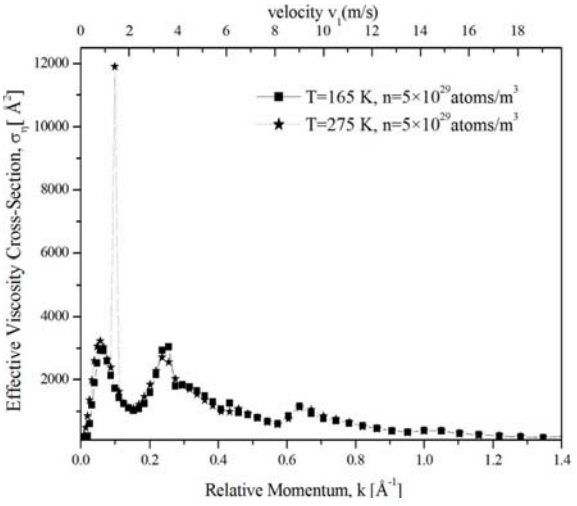

Figure 4. The effective viscosity cross section σ_η [Å^2] for ^{132}Xe-^{132}Xe scattering as a function of relative momentum k [Å^{-1}] at temperature T = 165 K and 275 K for number density n= 5×10^{29} atoms/m^3

3. RESULTS AND DISCUSSION

3.1 Effective total and viscosity cross sections

To calculate the ℓ-sums in Eqs. (14) and (15) to an accuracy of 0.5% or better, then partial waves up to $\ell = 14$ needed to include; for $\ell > 14$, the effect of the potential becomes negligible, high respect to the repulsive longer-range angular-momentum barrier $\sim \frac{\ell(\ell+1)}{r^2}$.

Figs. 1-5 and Tables 1-3 describe briefly our results. The velocity v_1[m/s] of a projectile atom (v_1= constant × k) as a function of k [Å^{-1}], presents the upper scale in the figures. Whereas the constant is 14.15Å.m/s, and the target atom is at rest (v_2=0).

Figures 1 and 2 show σ_T and σ_η for ^{132}Xe-^{132}Xe scattering as functions of k at T = 165 K for different number densities n. It is noted that the effective cross sections for high n are less than for low n in the limit k→0: As n increases, quantum effects become more pronounced since the particles come closer to each other; so the effective scattering cross sections decrease. For high k, the cross sections are independent of n because of the overall repulsive effects. This is because, for high k (corresponding to the atoms coming closer to each other), the short-range part of the interaction dominates.

Figures 3 and 4 represent σ_T and σ_η as functions of k at n = 5 × 10^{29} atoms/m^3 for two different T. It is clear that the effective cross sections at high T are larger than

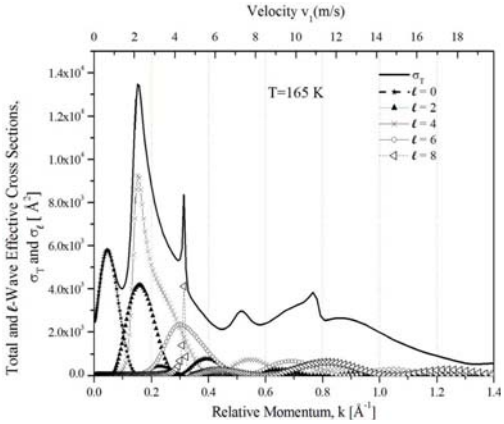

Figure 5. The ℓ -wave effective cross sections σ_ℓ [Å^2] for $\ell = 0,\ 2\ ,\ 4,\ 6,\ 8$ and the effective total cross section σ_T [Å^2] for ^{132}Xe-^{132}Xe scattering as functions of relative momentum k [Å^{-1}] for number density n= 1× 10^{21} atoms/m^3, using the HFD-B2 potential. The upper scale [m/s] represents the corresponding velocity v1 of a projectile atom on a stationary target atom

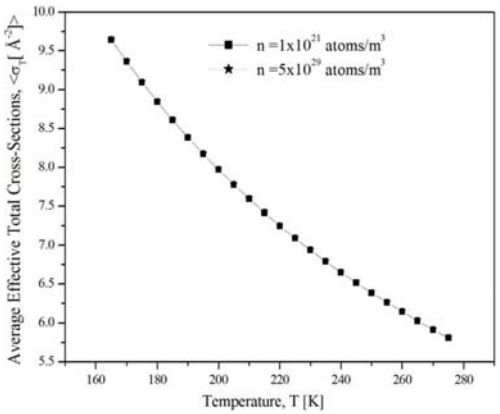

Figure 6. The average effective total cross section $\langle \sigma_T \rangle$ [Å^2] for ^{132}Xe-^{132}Xe scattering as a function of temperature T for two different number densities n

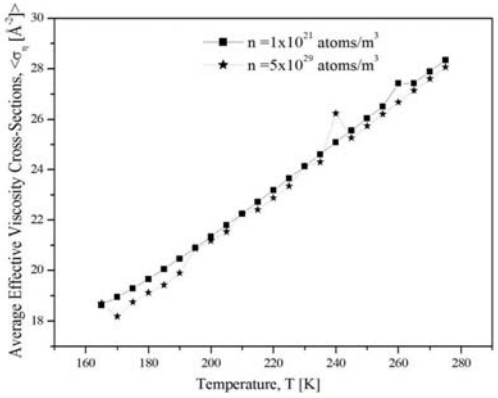

Figure 7. The average effective viscosity cross section $\langle \sigma_\eta \rangle$ [Å^2] for ^{132}Xe-^{132}Xe scattering as a function of temperature T for two different number densities n

for low T in the limit k→0 because of the overall disruptive effects of T. With increasing T, the atoms hop away from each other; in the limit k→0, the long-range part of the interaction dominates.

Figure 5 shows the behavior of σ_T and σ_ℓ ($\ell = 0\ ,\ 2\ ,\ 4,\ 6,\ 8$) as a function of k at number density $n = 1\times 10^{21}$ atoms/m^3. The odd partial waves canceled in Bose-Einstein statistics [22] For k < 0.1 Å^{-1}, the σ_0 dominates. As k increases, the higher partial waves contribution of the scattering increases, especially the D and G-waves $(\ell = 2, 4)$. σ_0 shows decreasing with increasing k (increasing energy); but the higher partial-waves contribute against this decrease, the most distinct being the D-wave. σ_2 and σ_4 initially increases with k> zero before passing through a maximum, and then tend to decrease. The peak in σ_T arises mainly from σ_2, and σ_4 which referrers to a quasi-bound state trapped by the $\ell = 2$, $\ell = 4$ angular-momentum barriers; this resonance occurs at k ~ 0.15188 Å^{-1} (for $n = 1\times 10^{21}$ atoms/m^3). Other peaks are very small; so their resonance contribution is negligible. Table 1 displays the relative momentum k$_r$, and σ_T at the resonance peaks. Table 2 displays the Ramsauer Townsend effect [22] where σ_T is a minimum; so that the atoms propagate through the medium almost freely.

The effective S-wave scattering length a$_o$, $\sigma_T(0)$, and $\sigma_\eta(0)$ were also calculated, as shown in Table 3. These are consistent with the values obtained from the well-known sum rules in the low T limit, where only small values of v1 are important:

$$\sigma_T(k) \underset{k\to 0}{\to} 8\pi a_o^2; \tag{16}$$

$$\sigma_\eta(k) \underset{k\to 0}{\to} \frac{16}{3}\pi a_o^2 \ . \tag{17}$$

The average effective total cross section and average effective viscosity cross section are given by [23]

$$\langle\sigma\rangle = (K_\beta T)^{-(p+1)} \int_0^\infty \sigma(E) E^P e^{(-E/K_\beta T)} dE\,. \tag{18}$$

When p = 1, this gives $\langle \sigma_T \rangle$; but for p = 3, $\langle \sigma_\eta \rangle$ is obtained.

Figures 6 and 7 indicate that $\langle \sigma_T \rangle$ decreases with T, but

Table. 1 The relative momentum k_r and total scattering cross section σ_T at the resonance peaks

ℓ	k_r[Å^{-1}]	σ_T (k_r) [Å^2]
0	0.04702	05.782×10^3
2,4	0.15188	13.462×10^3
6,8	0.31454	08.370 ×10^3

Table. 2 The Ramsauer Townsend relative momentum k_{min} and total scattering cross section σ_T

ℓ	k_{min}[Å^{-1}]	σ_T (k_{min}) [Å^2]
0	0.09815	04.010×10^3
4	0.44909	02.130 ×10^3

Table. 3 The effective S-wave scattering length a_o[Å], $\sigma_T(0)$ [Å^2] and $\sigma_\eta(0)$ [Å^2]

a_o[Å]	$\sigma_T(0)$ [Å^2]	$\sigma_T(k)_{k\to 0} 8\pi a_o^2$ [Å^2]	$\sigma_\eta(0)$ [Å^2]	$\sigma_\eta(k)_{k\to 0} \frac{16}{3}\pi a_o^2$ [Å^2]
9.3809	2211.6	2211.7	1474.4	1474.5

do not show a tangible change with n; while $\langle\sigma_\eta\rangle$ shows such a change for high n; thus because $\langle\sigma_T\rangle$ depends particularly on particle energies while $\langle\sigma_\eta\rangle$ depends on the transport angular momentum that is precisely affected by density.

4 . Conclusion

In this paper, extensive results for the effective total, viscosity and average cross sections for ^{132}Xe-^{132}Xe scattering in xenon gas are presented for temperatures 165K and 275 K. The calculations were based on the effective phase shifts determined within the GMF formalism. The resonance peaks energy is calculated and shows that the greatest demonstrate on σ_T comes from S-wave, while the other peaks come from D, G- waves. Ramsauer Townsend effect also displayed.

Acknowledgment

Conflict of Interest: The author declares that he has no conflict of interest.

References

1. RF Bishop, HB Ghassib, and MR Strayer. Low-Energy He-He Interactions with Phenomenological Potentials. *Journal of Low Temperature Physics*; **26** (1977) 669.
2. BR Joudeh, AS Sandouqa, and HB Ghassib. Al-Sugheir MK. ^{3}He-^{3}He and ^{4}He-^{4}He Cross Sections in Matter at Low Temperature. *Journal of Low Temperature Physics*; **161** (2010) 348.
3. IF Al-Maaitah, Total and Viscosity Cross Sections for Krypton Gas at Boiling Point. *Applied Physics Research*; **11** (2019) 88.
4. IF Al-Maaitah, Quantum Second Virial Coefficients for Krypton-86 gas. *Applied Physics Research*; **10** (2018) 1.
5. MC Bordage, SF Biagi, L L Alves, K Bartschat, and S Chowdhury *et al.* Comparisons of sets of electron–neutral scattering cross sections and swarm parameters in noble gases: III. Krypton and xenon. *Journal of Physics D Applies Physics*; **46** (2013) 334003.
6. M Hayashi, Determination of electron-xenon total excitation cross-sections, from threshold to 100 eV from experimental values of Townsend's α. *Journal of Physics D Applies Physics*; **16** (1983) 581.
7. P S Krstić and DR Schultz, Elastic and related transport cross sections for protons scattering from the noble gases He, Ne, Ar, Kr, and Xe. *Physics of Plasmas*; **13** (2006) 053501.
8. VE Krohn and G R Ringo, Measurement of the Electron-Neutron Interaction by the Asymmetrical Scattering of Thermal Neutrons by Noble Gases. *Physical Review Journals Archive*; **148** (1966) 1303.
9. I Amdu and E A Mason, Scattering of High Velocity Neutral Particles. VII. Xenon—Xenon. *The Journal of Chemical Physics*; **25** (1956) 624.
10. R S Robinson, Energetic binary collisions in rare gas plasmas. *Journal of Vacuum Science and Technology*; **16** (1979) 185.
11. AK Dham, W J Meath, A R Allnatt, R A Aziz and M Slaman, XC and HFD-B Potential Energy Curves for Xe-Xe and Releted Physical Properties. *Chemical Physics*; **142** (1990) 173.
12. G Fekete, Phonon Spectra and Thermodynamic Properties of Rare Gas Solids Based on Empirical and Semi-empirical (ab initio) Two-body Potentials: A Comparative Study. Msc Thesis, Brock University, (2004).
13. JM Standard and PR Certain, Bounds to two□ and three□body long□range interaction coefficients for S□state atoms. *The Journal of Chemical Physics*; **83** (1985) 3002.
14. M Alexandr and M Anatol, Monte Carlo Simulations of Thermodynamic Properties of Argon, Krypton and Xenon in Liquid and Gas State Using New *ab initio* Pair Potentials. Molecular Physics; **101** (2003) 3335.
15. F Michael and J Z Bruno, Computation of the Transport Coefficients of Dense Fluid Neon, *Argon, Krypton and Xenon by Molecular Dynamics. Molecular Physics*; **73** (1991) 471.
16. A V Phelps, *Collision Cross Sections for Identical and Non-Identical Rare-Gas Atom Pairs for Energies from 0.01 eV to 10 keV*. Boulder, Colorado :

University of Colorado and National Institute of Standards and Technology, (2004) 80309.
17. AM Ratner, Atoms and the Simplest Atomic Crystals. *Physics Reports*; **269** (1996) 197.
18. A Fetter AL and JD Walecka, *Quantum Theory of Many-Particle Systems*. New York: McGraw-Hill, (1971).
19. HB Ghassib, RF Bishop and MR Strayer, A Study of the Galitskii- Feynman T Matrix for Liquid ^{3}He. *Journal of Low Temperature Physics*; **23** (1976) 393.
20. M Lee, *Interaction in Low-Dimensional Bose-Einstein Condensates*, *Ph.D.* The University of Oxford, UK, (2002).
21. HT Stoof, M Bijlsma and M Houbiers, Theory of Interacting Quantum Gases. *Journal of Research of NIST*; **101** (1996) 443.
22. J P Aldridge and R H Davis, Calculated Ramsauer-Townsend effect in ^{4}He-^{4}He. *Physical Review Letter*; **19** (1967) 1001.
23. MJ Jamieson, A Dalgarno and J Yukich, *Elastic Scattering of Hydrogen Atoms at Low Temperatures. Physical Review A*; **46** (1992) 6956.